A Thermalization Energy Analysis of the Threshold Voltage Shift in Amorphous Indium Gallium Zinc Oxide Thin Film Transistors under Simultaneous Negative Gate Bias and Illumination

A. J. Flewitt [1,a] and M. J. Powell [2]

1. Electrical Engineering Division, Cambridge University, J J Thomson Avenue, Cambridge CB3 0FA, UK

2. 252, Valley Drive, Kendal, LA9 7SL, UK

Receipt date: 1 November 2013

Revised version: 19 March 2014

ABSTRACT

It has been previously observed that thin film transistors (TFTs) utilizing an amorphous indium gallium zinc oxide (a-IGZO) semiconducting channel suffer from a threshold voltage shift when subjected to a negative gate bias and light illumination simultaneously. In this work, a thermalization energy analysis has been applied to previously-published data on negative bias under illumination stress (NBIS) in a-IGZO TFTs. A barrier to defect conversion is extracted of 0.65 – 0.75 eV, which is consistent with reported energies of oxygen vacancy migration. The attempt-to-escape frequency is extracted to be 10^6 – 10^7 s^{-1} which suggests a weak localization of carriers in band tail states over a 20 – 40 nm distance. Models for the NBIS mechanism based on charge trapping are reviewed and a defect pool model is proposed in which two distinct distributions of defect states exist in the a-IGZO band gap: these are associated with states that are formed as neutrally charged and 2+ charged oxygen vacancies at the time of film formation. In this model, threshold voltage shift is not due to a defect creation process, but to a change in the energy distribution of states in the band gap upon defect migration as this allows a state formed as a

[a] Author to whom correspondence should be addressed. Electronic address: ajf@eng.cam.ac.uk .

neutrally charged vacancy to be converted into one formed as a 2+ charged vacancy and vice versa. Carrier localization close to the defect migration site is necessary for the conversion process to take place, and such defect migration sites are associated with conduction and valence band tail states. Under negative gate bias stressing, the conduction band tail is depleted of carriers, but the bias is insufficient to accumulate holes in the valence band tail states, and so no threshold voltage shift results. It is only under illumination that the quasi Fermi level for holes is sufficiently lowered to allow occupation of valence band tail states. The resulting charge localization then allows a negative threshold voltage shift, but only under conditions of simultaneous negative gate bias and illumination, as observed experimentally as the NBIS effect.

I. INTRODUCTION

Hydrogenated amorphous silicon (a-Si:H) has dominated as the material of choice for the channel semiconductor in thin film transistors (TFTs) for display backplanes for over two decades.[1] This is due to the exceptional uniformity which can be achieved in material properties over very large areas as a result of the amorphous microstructure. However, the inherently low electron mobility and metastability of a-Si:H means that it is becoming increasingly more difficult for this material to meet the ever-increasing demands of the display industry as it moves from liquid crystal to organic light emitting diode technology and with requirements for larger areas and higher resolutions. A number of alternative material systems to a-Si:H have emerged, including organic semiconductors,[2] nanocrystalline silicon, polycrystalline silicon and amorphous oxide semiconductors (AOSs).[3] Of these, AOSs are emerging as the preferred technology by the display industry with amorphous indium gallium zinc oxide (a-IGZO) being the most widely used channel semiconductor in combination with a silicon dioxide gate dielectric.[4] The amorphous microstructure immediately means that a-IGZO is equally well suited to large-area electronics as a-Si:H, but retains a high electron mobility (>10 $cm^2 V^{-1} s^{-1}$) due to the spherical symmetry of the overlapping metallic s electron states that form the bottom of the conduction band.[5]

Particular attention has been paid to the stability of a-IGZO TFTs under a variety of bias stress conditions.[6] The change in carrier density in the channel of a semiconductor upon application of a bias to the gate with respect to the source, V_{GS}, can result in a number of microscopic processes taking place including charge trapping in the dielectric, charge trapping at the interface between the dielectric and semiconductor, and a change in the defect distribution in the semiconductor. Depending on which processes are taking place, the effect on the transfer characteristics of the TFT may be a shift in the threshold voltage, V_{th}, or a change in the sub-threshold slope, or a change in the field-effect mobility, μ_{FE}, or some combination of these.

A number of studies have focussed particularly on the effect of negative bias stress ($V_{GS} < V_{th}$) as TFTs are actively driven to negative gate voltages during normal operation of a display backplane.[7-10] Of note is that, whilst almost no change in TFT transfer characteristics is observed under negative bias stress in the dark, if the TFT is subjected to illumination with a photon energy approaching that of the band gap of the a-IGZO (~3 eV) then a shift in V_{th} to more negative voltages is observed. The recent study of this 'negative bias under illumination stress' (NBIS) by Chowdhury *et al.* is particularly interesting, [8] as the authors measure the effect of temperature on this process, and this permits an analysis based on the concept of the thermalization energy which has previously been applied to amorphous, microcrystalline and polycrystalline silicon TFTs.[11-13]

In this work, such a thermalization energy analysis is applied to NBIS data of Chowdhury *et al*.[8] The parameters from this analysis are compared with previous studies on the stability of a-Si:H TFTs. It is clear that a very different microscopic mechanism is responsible for the threshold voltage shift in a-IGZO TFTs. Previously-published models for the NBIS mechanism are reviewed in the light of this thermalization energy analysis. A study of the threshold voltage shift in multicomponent oxide TFTs by Jackson *et al.* comparing TFTs different dielectrics concluded that charge trapping in the dielectric was unlikely to be responsible for this process as the threshold voltage shift was

independent of the dielectric employed [10]. Therefore, most recent studies have concluded that oxygen vacancies play a dominant role in the NBIS mechanism.[6,8,14,15]

With reference to previously published work on the nature of oxygen vacancies, it is postulated that two distinct distributions of oxygen vacancy states must exist in the band gap of a-IGZO which are in thermal equilibrium, and where the Fermi energy affects this equilibrium. This is analogous to the Defect Pool Model that was previously developed for a-Si:H.[16-18] A microscopic model which allows this equilibrium to change is proposed which is based on an oxygen vacancy defect migration (rather than defect creation) process. The oxygen vacancy migration model is shown to be consistent with previous work on the physics of oxygen vacancies and clearly explains why light illumination is required for a threshold voltage shift to occur under negative bias but not positive bias in a-IGZO TFTs.

II. THERMALIZATION ENERGY ANALYSIS

The starting point for the thermalization energy concept is that a material contains a number of sites which may be converted into defects by some means when the material is in an equilibrium state. No assumptions are required about the mechanism for the defect conversion process, but simply that each potential defect site will have a particular energy barrier to becoming the site of a defect resulting in the whole material having a distribution of energy barriers to defect conversion, $D(E)$. If an attempt-to-escape frequency, ν, is defined as being the number of times per second that an attempt is made to overcome the barrier to converting a particular site to a defect, then if the material is subjected to a change (e.g. a gate bias) such that it is no longer in equilibrium at some time $t = 0$, then after some time t, Boltzmann statistics shows that it is statistically likely that all potential defect sites $D(E)$ with an energy less than $k_B T \ln(\nu t)$ will have been converted into defects, where T is the temperature and k_B is the Boltzmann constant. As it takes a longer time to convert defect sites with a higher energy, time may be converted directly into a thermalization energy, E_{th}, where

$$E_{th} = k_B T \ln(\upsilon t) \,, \tag{1}$$

allowing $D(E)$ to be determined.[19] The beauty of the thermalization energy lies in the fact that the approach is agnostic to the defect conversion mechanism and has only one fitting parameter in the attempt-to-escape frequency.

The attempt-to-escape frequency may be evaluated by performing the same experiment at a number of different temperatures. If it is assumed that the distribution $D(E)$ does not change with temperature, which is reasonable if the temperature change does not lead to some structural change in the material, then when the correct ν is chosen, all measurements of the effect of the conversion of sites to defects should lie on the same line when plotted as a function of thermalization energy. The data presented by Chowdhury *et al.* [8] allows this analysis to be performed for NBIS.

Chowdhury *et al.* study a bottom gate inverted structure a-IGZO TFT with a 200 nm thick silicon dioxide gate dielectric.[8] The TFT is subjected to NBIS with V_{GS} = –20 V under a 3.4 eV photon illumination of 0.7 mW cm^{-2} intensity at temperatures between 303 K and 343 K, and gate transfer characteristics are measured periodically at each temperature to determine the threshold voltage shift as a function of stressing time $\Delta V_{th}(t)$. The authors fit their data to a stretched exponential function

$$|\Delta V_{th}(t)| = [V_{th}(\infty) - V_{th}(0)]\left[1 - \exp\left(\left[-(t/\tau)\right]^{\beta}\right)\right], \tag{2}$$

where $V_{th}(0)$ and $V_{th}(\infty)$ are the threshold voltage before stressing and the threshold voltage that the device is tending towards for long stressing times respectively, τ is a time constant and β is the exponential stretch parameter. For simplicity, in this work the normalized threshold voltage shift $\Delta V_n(t)$ will be defined as being

$$\Delta V_n(t) = |\Delta V_{th}(t)| / [V_{th}(\infty) - V_{th}(0)] \,, \tag{3}$$

so that (2) reduces to

$$\Delta V_n(t) = 1 - \exp\left(\left[-(t/\tau)^{\beta}\right]\right). \quad (4)$$

Figure 1 shows the result of replotting the fitted stretched exponential ΔV_n functions from Table I of Ref. 8 as a function of thermalization energy rather than time for three different attempt-to-escape frequencies: 10^5 s^{-1}, 10^6 s^{-1}, and 10^7 s^{-1}. All $\Delta V_n(E_{th})$ curves should overlap independent of NBIS temperature at the correct ν for the defect conversion process that is operating. From Fig. 1, it is clear that a reasonable overlap does occur for ν ~ 10^6 to 10^7 s^{-1}. However, alignment is not perfect due to a combination of the fact that the stretched exponential is rarely a good fit to stress data for longer stress times,[13] and the repeated interruption of the NBIS process to perform gate transfer measurement of V_{th} which acts as a perturbation.

By substituting E_{th} for t in (4) using (1) for the thermalization energy, it is possible to write the stretched exponential as

$$\Delta V_n(E_{th}) = 1 - \exp\left(-\left[\nu\tau\right]^{-\beta} \exp\left[\beta E_{th}/k_B T\right]\right). \quad (5)$$

This is also plotted in Fig. 1 as a line without symbols at each attempt-to-escape frequency for the 343 K stretched exponential data. Differentiating this curve then allows the form of the distribution of energy barriers to defect conversion, $D(E)$, to be determined, and this is plotted for attempt to escape frequencies of 10^6 s^{-1} and 10^7 s^{-1} in Fig. 2. Allowing for the uncertainty in the determination of the attempt-to-escape frequency, this shows that $D(E)$ has a peak at E_{max} between 0.65 and 0.75 eV and a full width at half maximum ~0.25 eV. It should be noted that this analysis is fundamentally different to that applied by Chowdhury *et al*. in that a distribution of energy barriers is being extracted in this analysis rather than an attempt to fit the data to a single energy barrier, which is not physically realistic.

It is now possible to extend the previous comparative study of the positive bias stress (PBS) stability of amorphous, microcrystalline and polycrystalline silicon TFTs made by Wehrspohn *et al.* [11] to NBIS in a-IGZO. It should be noted that a stretched hyperbola is used to fit stressing data by Wehrspohn *et al.* of the form

$$\left|\Delta V_{th}(E_{th})\right| = \left[V_{th}(\infty) - V_{th}(0)\right]\left[1 - \left(1 + \exp\left[\left(E_{th} - E_A\right)/k_B T_0\right]\right)^{-1/\varepsilon}\right], \qquad (6)$$

where $\varepsilon \approx 0.5$.[20] This has two fitting parameters: $k_B T_0$ which is a measure of the width of $D(E)$, and E_A which is related to E_{max} by

$$E_{max} = E_A - k_B T_0 \ln 2 \ . \qquad (7)$$

Table I in this work is therefore adapted from Table I in Ref. [11] where E_{max} is included rather than E_A.

III. REQUIREMENTS OF THE NBIS INSTABILITY MECHANISM

In the light of this thermalization energy analysis and previous studies, any model that attempts to explain the NBIS instability mechanism must explain the following essential details:

1. a negative shift in the threshold voltage occurs for negative gate bias and a positive shift occurs for positive gate bias;

2. illumination with light is required to induce a negative threshold voltage shift, whereas positive threshold voltage shifts occur both with and without illumination;

3. the threshold voltage shift is metastable (i.e. the effect is persistent after the removal of the gate bias), and the rate of shift is strongly temperature-dependent in the range from room temperature up to 373 K when structural changes are not occurring;

4. the energy barrier to the instability mechanism is 0.65 – 0.75 eV; and

5. there is an attempt-to-escape frequency of 10^6 – 10^7 s^{-1} associated with the instability process.

Models for the threshold voltage shift in TFTs fall generically into three categories:

1. those that involve charge trapping in the gate dielectric;

2. those that involve charge trapping in existing states in the semiconducting channel; and

3. those that involve some change in the distribution of gap states in the semiconducting channel.

Ascribing a mechanism to a measured threshold voltage shift is not straightforward, as there will be dependence on the quality of the dielectric and semiconductor and also on the magnitude of the gate electric field. This discussion is restricted to TFTs incorporating a high quality, wide bandgap dielectric and low defect density semiconductor, under gate electric fields common in the practical use of TFTs in displays ~1 MV cm^{-1}. This is the case for the silicon dioxide, a-IGZO and –20 v bias employed by Chowdhury *et al.* [8]

Jackson *et al.* have previously concluded that threshold voltage shifts under negative gate bias in multicomponent oxide TFTs is unlikely to be due to charge trapping in the dielectric as the process appears to be independent of the dielectric employed.[10] Furthermore, the offset between the valence mobility edge in a-IGZO and the valence band maximum in silicon dioxide is in excess of 1 eV.[21] As the 3.4 eV photon illumination is only sufficient to generate electron-hole pairs in the a-IGZO, and not directly in the dielectric, it is unlikely that holes will penetrate into the dielectric from the semiconductor. Neither is there any apparent correlation of such a mechanism with the energy barrier for the process or the attempt-to-escape frequency that has been extracted, nor a reason for the rate of threshold shift being strongly temperature-dependent when the hole trapping is entirely driven by an electric field in this mechanism. Therefore, a mechanism involving charge trapping in existing gap states or a change in the distribution of gap states is most likely.

In order for charge trapping in the a-IGZO to be the NBIS mechanism, it is necessary for positive charge to be created close to the dielectric interface so that there is an effect on the threshold voltage. Photon illumination will clearly reduce the hole quasi-Fermi level so that positive

charge can be created in deep oxygen vacancy states. The positive charge needs to be separated from the generated electrons, and the applied gate field would provide a mechanism for this. However, it is again not clear why there should be a strong temperature dependence to this process and an energy barrier of 0.65 – 0.75 eV. An additional complexity therefore has to be introduced into such models such as vacancy diffusion,[21] or photonic energy barrier lowering.[8]

Therefore, for the remainder of this paper, the possibility of a model based on a change in the distribution of gap states is proposed, as found in other amorphous semiconductors with a significant number of tail states. It is shown that such a model fulfils all five of the requirements set out here, and explains positive bias stress also.

IV. OXYGEN VACANCY BAND GAP STATES

In comparing the data in Table I for the a-IGZO TFT under NBIS with PBS in the thin film silicon TFTs, it is notable that while E_{max} is of a comparable order to the thin film silicon case, it is actually slightly smaller. In the case of thin film silicon, it is the breaking of a weak Si—Si bond that is the rate limiting step to defect creation in PBS and this leads to the fairly consistent E_{max} = 1.0 eV across the range of materials and devices.[18] It has been suggested that oxygen vacancy (V_O) states lying deep in the band gap (~1 eV above the valence band mobility edge E_V) are responsible for instabilities in a-IGZO TFTs.[14] The modeling of defect states in amorphous materials by techniques such as density functional theory is notoriously difficult due to the need to generate an arrangement of atoms that realistically represents an amorphous structure with the required defect state present. However, there have been such studies on crystalline ZnO, and there is a consensus that the energy for neutral V_O creation is between 0.85 and 1.0 eV when the Fermi energy is in the upper half of the band gap ($E_F - E_v > 2.2$ eV), as is the case for these intrinsically n-type materials.[22-24] If the Fermi energy drops lower in the band gap, then the formation energy of an oxygen vacancy with a 2+ charge (V_O^{2+}) becomes lower than the formation energy of an uncharged oxygen vacancy (V_O).[22]

For the remainder of this work, defects *formed* in the (uncharged) V_O state will be referred to as D_e states, as they will tend to be formed under conditions of electron accumulation. Defects formed as V_O^{2+} states, which will tend to be under hole accumulation, will be referred to D_h states, in analogy with the Defect Pool Model notation used previously for considering defects in a-Si:H TFTs.[16] Density functional theory (DFT) calculations on D_e states in IGZO suggest that they form a band of mid-gap states ~1.1 eV above the valence band mobility edge.[25] As the D_h states are, by definition, in a 2+ charge state, their electron occupancy is low, and so they must be at a higher energy in the density of states than the D_e states, and this is shown in the schematic diagram of the a-IGZO density of states in Fig. 3(a). After formation, both D_e and D_h states may be either neutrally charged or doubly charged (the single charge condition being unstable due to the energy gain from lattice contraction) depending on the position of the Fermi level at a particular moment in time.

Clearly, defect states will be formed during the deposition of an a-IGZO thin film. If no further structural change in the material is possible, then this implies that the density of states of D_e and D_h oxygen vacancies is fixed for all time. However, it is known that diffusion of oxygen vacancy states does occur in metal oxides, and this process has been modelled in both crystalline zinc oxide,[26] and crystalline indium oxide.[27] Therefore, if a particular oxygen vacancy migrates from one site in the continuous random network in a-IGZO to another neighbouring site, then the Fermi energy at that time and the local structure and charge availability will determine whether the new site is a D_e or D_h state (i.e. the state in the new defect site is not necessarily the same as that at the old defect site). Therefore, defect migration provides a means by which the density of states in the band gap of IGZO may change without the need for some macroscopic structural change, as might occur at high temperatures. This is also consistent with recent experimental evidence of oxygen diffusion into a-IGZO thin films from an oxygen-rich surface,[28] and with the long-standing belief that the overall oxygen vacancy density does not change upon bias stressing of an a-IGZO TFT (i.e oxygen vacancy defects are not created by release of an oxygen atom from a potential defect creation site, which would be analogous to defect creation in a-Si:H TFTs under bias stress).[29]

V. CHARGE LOCALIZATION NEAR DEFECTS

The second key parameter in Table I is the attempt-to-escape frequency. If this is considered simply to be the number of times per second that an attempt is made to migrate an oxygen vacancy site within the a-IGZO network, then it might be expected that this should correspond to typical phonon frequencies ~10^{13} s^{-1}. However, Table I shows that such high values of ν are not observed in the defect conversion process, and this is because a charge carrier (electron or hole) has to be localised at the potential defect formation site if migration with a change of state (from D_e to D_h or vice versa) is to be permitted. In a-Si:H, it is the weak bonds in the band tails that are the potential defect sites. Electrons in these band tail states are localised within ~2 nm of the potential defect site, and so Wehrspohn *et al.* argue that this represents ~10^3 increase in the volume of space occupied by such an electron compared with one localised completely within a bond; the 10^{13} s^{-1} phonon frequency is reduced by 10^3 to give an attempt-to-escape frequency of ~10^{10} s^{-1}, as observed experimentally.[11] Bottom gate μc-Si:H TFTs have a similar attempt-to-escape frequency to a-Si:H as the microcrystalline layer is highly defective and has a significant amorphous fraction in the incubation layer close to the gate dielectric where charge accumulation occurs, and so the electron localisation length is also very similar. Top gate μc-Si:H TFTs, however, form an accumulation layer in a region where the crystallites are relatively large and the amorphous fraction is low. It is for this reason that top gate μc-Si:H TFTs have a consistently higher field effect mobility than equivalent bottom gate TFTs. Electrons are now localised to within grains which are typically ~10 to 20 nm in diameter. The further 10^3 increase in volume of space occupied by these localised electrons compared with the a-Si:H case results in a further decrease in the attempt-to-escape frequency by the same order to ~10^7 s^{-1}.[11] It is important to note that top gate μc-Si:H TFTs are significantly more stable than bottom gate TFTs not because the energy for defect creation is higher, but because the attempt-to-escape frequency has been greatly reduced, and this variation is possible even within the same material.

In the a-IGZO under NBIS, the attempt-to-escape frequency is observed to be between 10^6 and 10^7 s^{-1}. This suggests that carriers are localised around potential defect sites in a volume of space that is a factor of $10^6 – 10^7$ larger than a single bond. The metal—O bond length in crystalline a-IGZO is ~0.2 nm,[30] and so the attempt-to-escape frequency suggests a localisation length around the defect migration site of ~20 – 40 nm. Fig. 3(a) shows a schematic diagram of the density of states in a-IGZO. Conduction in a-IGZO is dominated at low carrier densities by weakly localized electrons moving between the conduction band tail states in a trap-limited conduction mechanism.[29,31] The attempt-to-escape frequency would suggest that this localization length is ~20 – 40 nm. Such spatial localization of carriers in band tail states is consistent with the Anderson model for disordered solids.[32] Calculation of the localization length in a particular disordered material is not trivial, [33] and there is no published data for the carrier localization length in a-IGZO. However, the localization length should be greater than the mean free path (~1 nm in a-IGZO) and less than the Debye length (in excess of 100 nm).[31] This is exactly the situation in microcrystalline silicon TFTs.[11]

In the recent study of Hall mobility in a-IGZO by Kamiya *et al.*, [34] a percolation conduction mechanism is presented which supports this view of carrier localization in a-IGZO. In the percolation conduction mechanism, the potential wells in which carriers are localized have a significantly longer length than the 1 nm mean free path. This is required in order to explain the absence of an anomalous Hall effect in this disordered material despite a $T^{-1/4}$ dependence of conductivity with temperature. Therefore, the localization length extracted through the thermalization energy analysis is consistent with the Kamiya percolation conduction mechanism.

VI. OXYGEN VACANCY MIGRATION MODEL

A Defect Pool Model of the NBIS process now begins to emerge. The key features of the Defect Pool Model are that there should be some thermally equilibrated distribution of defect states in an amorphous material, where the inherent disorder leads to a broad energy density of states

distribution of defect states. These conditions appear to me met in a-IGZO where the equilibration of the defect distribution is achieved through oxygen vacancy migration. If this is the case, then it would be expected that the distribution of energies barriers for defect conversion determined by the thermalization energy analysis of NBIS shown in Fig. 2 should correlate with the energy barrier for oxygen vacancy migration in a-IGZO. Although there are no direct experimental measurements of this, *ab initio* modelling of these energy barriers in crystalline zinc oxide and crystalline indium oxide shows that they are significantly dependent on the charge state of the defect site, and can be as low as 1.09 eV in zinc oxide and 0.71 eV in indium oxide when the vacancy is in the 2+ charge state. Therefore, given the amorphous structure and variety of metal cations in a-IGZO, the distribution of defect conversion energies around 0.65 – 0.75 eV extracted for NBIS is consistent with this process.

This leads to postulation of the following microscopic model of the processes to allow an interchange between D_e and D_h states upon vacancy migration:

$$D_e + [O(—M)_n + 2h] \rightarrow D_e + O_i + D_h^{2+} \rightarrow O(—M)_n + D_h^{2+} \quad (8a)$$

$$D_h^{2+} + [O(—M)_n + 2e] \rightarrow D_h^{2+} + O_i^{2-} + D_e \rightarrow O(—M)_n + D_e \quad (8b)$$

where O_i is an interstitial oxygen atom moving between defect sites and $O(—M)_n$ is an *n*-coordinated oxygen atom at a site neighbouring the oxygen vacancy to or from which migration will occur or has occurred. $[O(—M)_n + 2e]$ represents electron localization close to such a site and $[O(—M)_n + 2h]$ represents similar hole localization. Figure 4 shows these two processes schematically.

Equation (8a) specifically represents the process of converting a D_e state to a D_h state upon oxygen vacancy migration. If a D_h state is formed upon vacancy migration then, by definition, it must have a 2+ charge at the time of formation, and an oxygen atom must now exist at the original oxygen vacancy site. This therefore determines the right hand side of Eqn. (8a). Before migration, the oxygen vacancy was a D_e state and therefore most likely to be occupied by electrons (uncharged). At some point, an oxygen atom must move between the new and old defect sites,

going through an O_i interstitial site – this is the barrier to defect migration. When the oxygen atom is in the interstitial state, both the old D_e vacancy and the new D_h^{2+} vacancy must exist as well, and this determines the middle of Eqn. (8a). Charge conservation shows that the O_i must be uncharged in this process, and also that the localization of two holes is required on the left hand side of Eqn. (8a) for the process to occur. A similar argument applies to Eqn. (8b), where the new D_e state must be uncharged upon formation, the old D_h state is most likely to be positively charged, the oxygen interstitial must be in a 2– ionized state and localization of two electrons is required for the process to occur. It should be noted that charge localization is not required for simple defect migration where both the old and new defect sites are of the same state. Also, it is the distinction between the D_e and D_h states which results in metastability – that there is an inherent difference in the position in the band gap of a defect state that is *formed* in a charged (relaxed) compared with an uncharged (unrelaxed) condition upon migration – and the importance of the band tail states as charge localization sites to which defects are likely to migrate due to local network disorder.

There are several notable features of this model. First is the consistency with the thermalization energy analysis of NBIS in Section II. There is a clear barrier to defect conversion in the formation of the O_i site, and the energy extracted is consistent with published calculations. Also, as carriers are only weakly localized around these defect migration sites, the attempt-to-escape frequency is reduced from the phonon frequency to between 10^6 and 10^7 s^{-1}, as extracted. Second is the consistency with experimental data on bias stressing of a-IGZO TFTs. Under simple positive gate bias stress, more electrons are localized on conduction band tail states, so (8b) is favoured while (8a) is suppressed due to the lack of localized holes in the valence band tails. More D_e states will be created at the expense of D_h states, and this will pull the Fermi level lower in the band gap when the gate bias is removed, leading to an increased threshold voltage as observed experimentally. Under simple negative gate bias, the conduction band tails are depleted of electrons, suppressing (8b). However, as the bias is insufficient to pull the Fermi energy down through the large number of D_e states, the localized valence band tail states can never be accumulated with holes, so (8a) is also

suppressed. Only under illumination with photons are holes in the valence band tail created, allowing the hole quasi Fermi level to be pulled towards the valence band. This permits (8a) and D_h states may be created at the expense of D_e states. Electrons are also being localised on the conduction band tail states and so (8b) is permitted, but the number of D_h^{2+} states is so small compared with the number of D_e states due to the energetics of their creation at film formation that the equilibrium is moved with the net result being more D_h state creation. This pulls the Fermi energy up towards the conduction band when the gate bias is removed. Therefore, it is only the *combination* of photon illumination with energies sufficient to lead to hole generation in valence band tail states *and* negative gate bias that will lead to the negative threshold voltage shift as observed experimentally. The consequence of this is that both sub-gap as well as band-gap illumination can produce the NBIS effect.

VII. CONCLUSIONS

A thermalization energy analysis has been applied to previously-published data on the threshold voltage shift in a-IGZO TFTs under negative gate bias and simultaneous illumination. A barrier to defect conversion of 0.65 – 0.75 eV and an attempt-to-escape frequency of $10^6 – 10^7$ s^{-1} are extracted. The former correlates with the energy barrier for oxygen vacancy migration in a-IGZO and the latter with a charge carrier localization length of 20 – 40 nm. Using this result, and with reference to other studies on the physics of defects in metal oxides, a microscopic model for the origin of the threshold voltage shift in a-IGZO TFTs is proposed as an alternative to charge trapping models which do not explain all of the NBIS phenomena. The key features of the model are that two distinct distributions of defect states exist in the band gap of a-IGZO: one associated with oxygen vacancies formed in the neutral charge state which lies towards the valence band (D_e states), and one associated with oxygen vacancies formed in the 2+ charge state which lies towards the conduction band (D_h states). Oxygen vacancy migration is an ever-present process in metal oxides. If appropriate charge is localized at the time of migration, then it is possible for a D_e state to be

converted to a D_h state and vice versa. A change in the electron and hole quasi Fermi energy therefore changes the equilibrium between the pool of D_e and D_h defect states, and this leads to a change in the threshold voltage of the TFT. Such a model provides not only a clear explanation of the NBIS effect in a-IGZO TFTs including when the photon energy is less than the band gap, but also of positive bias stress without illumination. It is likely that such a model could be applied to other amorphous oxide semiconductors.

ACKNOWLEDGEMENTS

The research leading to these results has received funding from the European Community's 7th Framework Programme under grant agreement NMP3-LA-2010-246334. Financial support of the European Commission is therefore gratefully acknowledged.

[1] A. J. Flewitt, in *Handbook of Visual Display Technology*, edited by J. Chen, W. M. Cranton, and M. Fihn (Springer, 2012), Vol. 1, pp. 628.

[2] A. C. Arias, J. D. MacKenzie, I. McCulloch, J. Rivnay, and A. Salleo, Chem. Rev. **110**, 3 (2010).

[3] E. Fortunato, P. Barquinha, and R. Martins, Adv. Mater. **24**, 2945 (2012).

[4] K. Nomura, H. Ohta, A. Takagi, T. Kamiya, M. Hirano, and H. Hosono, Nature **432**, 488 (2004).

[5] H. Hosono, J. Non-Cryst. Solids **352**, 851 (2006).

[6] J. F. Conley, IEEE Trans. Dev. Mater. Reliability **10**, 460 (2010).

[7] K. Nomura, T. Kamiya, Y. Kikuchi, M. Hirano, and H. Hosono, Thin Solid Films **518**, 3012 (2010).

[8] M. D. H. Chowdhury, P. Migliorato, and J. Jang, Appl. Phys. Lett. **102**, 143506 (2013).

[9] K. Nomura, T. Kamiya, M. Hirano, and H. Hosono, Appl. Phys. Lett. **95**, 013502 (2009).

[10] W. B. Jackson, R. Hoffman, B. Yeh, T. Emery, T. Koch, C. McConica, and O. Kwon, phys. stat. sol. (a) **207**, 695 (2009).

[11] R. B. Wehrspohn, S. C. Deane, I. D. French, and M. J. Powell, Thin Solid Films **383**, 117 (2001).

[12] R. B. Wehrspohn, S. F. Lin, A. J. Flewitt, W. I. Milne, and M. J. Powell, J. Appl. Phys. **98**, 054505 (2005).

[13] S. Deane, R. Wehrspohn, and M. Powell, Phys. Rev. B **58**, 12625 (1998).

[14] J. Robertson, J. Non-Cryst. Solids **358**, 2437 (2012).

[15] Y. Jeong, C. Bae, D. Kim, K. Song, K. Woo, H. Shin, G. Cao, and J. Moon, ACS Appl. Mater. Interfaces **2**, 611 (2010).

[16] M. J. Powell, C. van Berkel, A. R. Franklin, S. C. Deane, and W. I. Milne, Phys. Rev. B **45**, 4160 (1992).

[17] M. J. Powell and S. C. Deane, Phys. Rev. B **48**, 10815 (1993).

[18] M. J. Powell, S. C. Deane, and R. B. Wehrspohn, Phys. Rev. B **66**, 155212 (2002).

[19] M. Stutzmann, W. B. Jackson, and C. C. Tsai, Phys. Rev. B **32**, 23 (1985).

[20] R. B. Wehrspohn, S. C. Deane, I. D. French, I. Gale, J. Hewett, M. J. Powell, and J. Robertson, J. Appl. Phys. **87**, 144 (2000).

[21] B. Ryu, H. K. Noh, E. A. Choi, and K. J. Chang, Appl. Phys. Lett. **97**, 022108 (2010).

[22] S. J. Clark, J. Robertson, S. Lany, and A. Zunger, Phys. Rev. B **81**, 115311 (2010).

[23] S. Lany and A. Zunger, Phys. Rev. B **78**, 235104 (2008).

[24] F. Oba, A. Togo, I. Tanaka, J. Paier, and G. Kresse, Phys. Rev. B **77**, 245202 (2008).

[25] C. Chen, K. C. Cheng, E. Chagarov, and J. Kanicki, Jap. J. Appl. Phys. **50** (2011).

[26] P. Erhart and K. Albe, Phys. Rev. B **73**, 115207 (2006).

[27] P. Ágoston and K. Albe, Phys. Rev. B **81**, 195205 (2010).

[28] K. Nomura, T. Kamiya, and H. Hosono, ECS J. Solid State Sci. Technol. **2**, P5 (2013).

[29] J. Robertson, phys. stat. sol. (b) **245**, 1026 (2008).

[30] M. Orita, H. Tanji, M. Mizuno, H. Adachi, and I. Tanaka, Phys. Rev. B **61**, 1811 (2000).

[31] S. Lee, K. Ghaffarzadeh, A. Nathan, J. Robertson, S. Jeon, C. Kim, I.-H. Song, and U.-I. Chung, Appl. Phys. Lett. **98**, 203508 (2011).

[32] P. W. Anderson, Phys. Rev. **109**, 1492 (1958).

[33] B. Kramer and A. MacKinnon, Rep. Prog. Phys. **56**, 1469 (1993).

[34] T. Kamiya, K. Nomura, and H. Hosono, Appl. Phys. Lett. **96**, 122103 (2010).

[35] T.-C. Fung, C.-S. Chuang, C. Chen, K. Abe, R. Cottle, M. Townsend, H. Kumomi, and J. Kanicki, J. Appl. Phys. **106**, 084511 (2009).

	Type of stress	ν [s^{-1}]	E_{max} ± 0.05 [eV]
a-Si:H BG TFT	PBS	10^{10}	0.85 – 1.00
µc-Si:H BG TFT	PBS	10^{10}	1.00
µc-Si:H TG TFT	PBS	5×10^{6}	1.00
Poly-Si TG TFT	PBS	$10^{5} – 10^{6}$	No data
a-IGZO BG TFT	NBIS	$10^{6} – 10^{7}$	0.65 – 0.75

Table I. Comparison of the peak energy for defect conversion, E_{max}, and the attempt-to-escape frequency, ν, for thin film silicon TFTs under positive bias stress (PBS) based on the data in Ref. [11] and a-IGZO under NBIS.

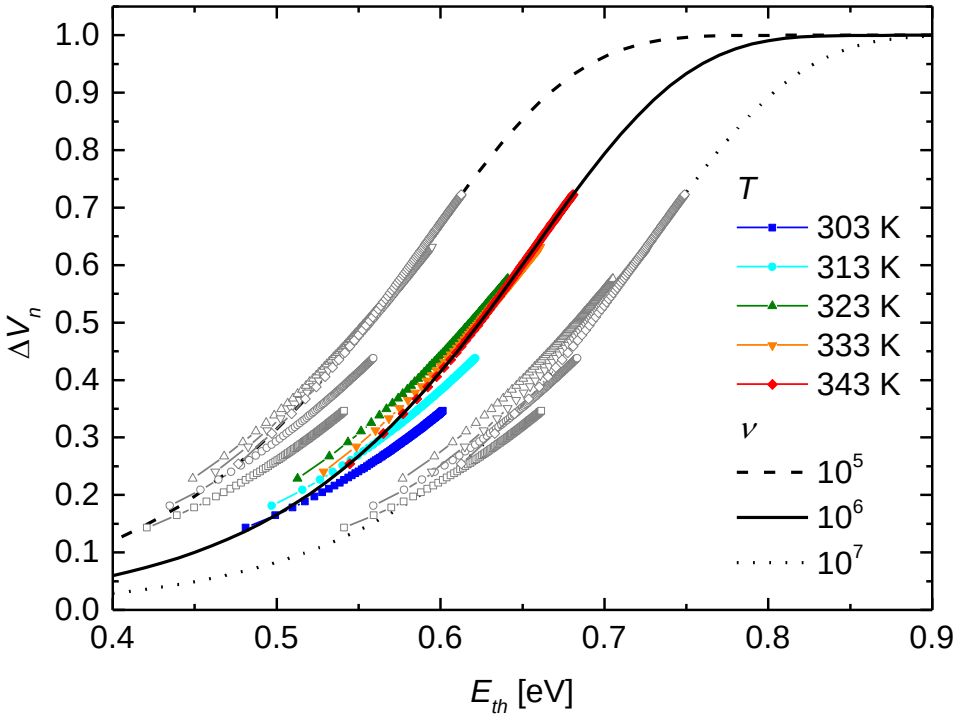

Fig. 1. The normalised threshold voltage shift, ΔV_n, replotted as a function of thermalization energy for the NBIS data at different stressing temperatures from Ref. 8 assuming attempt-to-escape frequencies of 10^5, 10^6 and 10^7 s^{-1}.

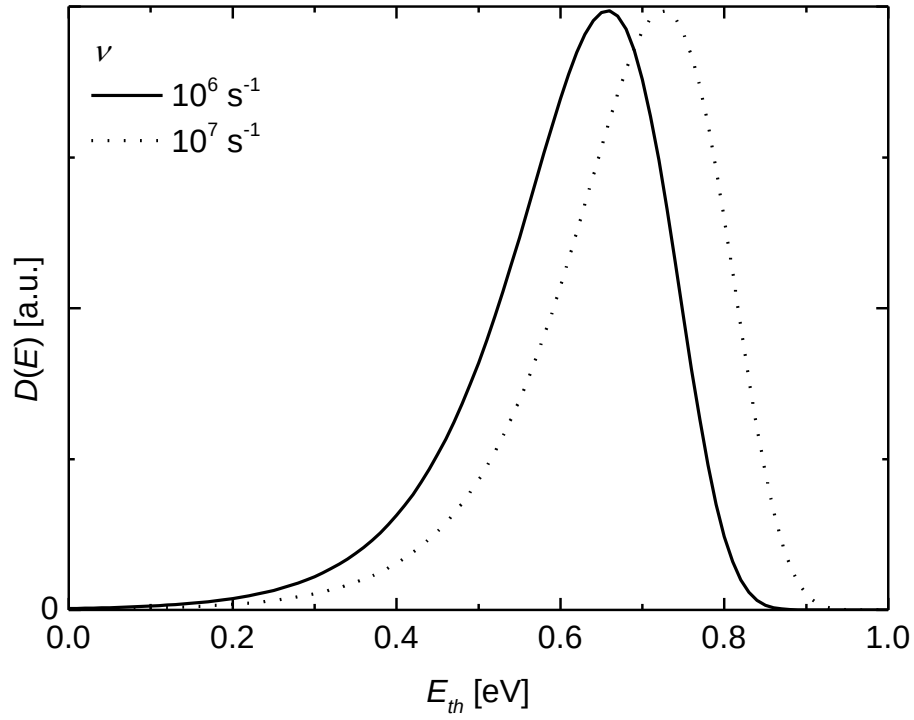

Fig. 2. The distribution of energy barriers to defect conversion, $D(E)$ calculated by differentiating the threshold voltage shift with respect to thermalization energy for attempt-to-escape frequencies of 10^6 and 10^7 s^{-1}.

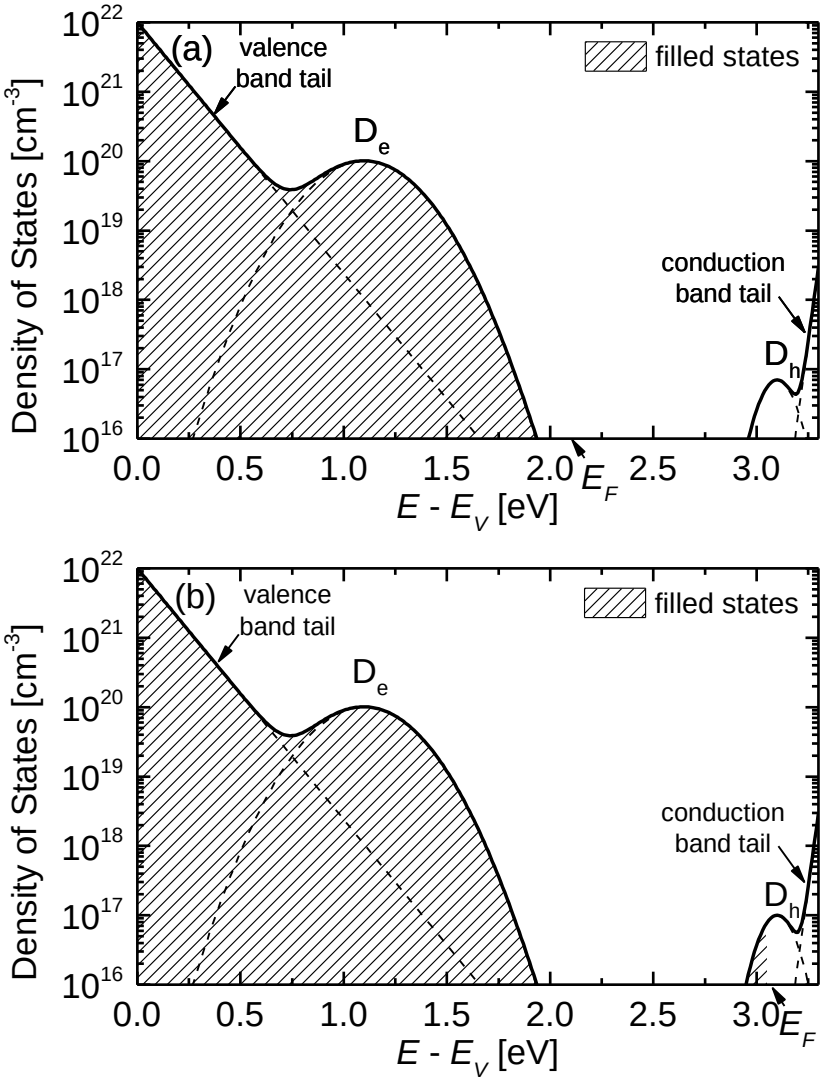

Fig. 3. (a) Schematic diagram of the density of states in as-deposited a-IGZO in the band gap (between the mobility edges) based on Refs. [14] and [35]. The separate contribution of the band tails and oxygen vacancy states are shown as dashed lines towards the total density of states shown as a solid line. Filled states under conditions of no gate bias are shown as being hatched. (b) Schematic diagram of the density of states in a-IGZO after NBIS. The density of D_e states has been reduced whilst the D_h states have increased by the same amount, resulting in the Fermi level moving to a higher position in the band gap upon removal of the gate bias.

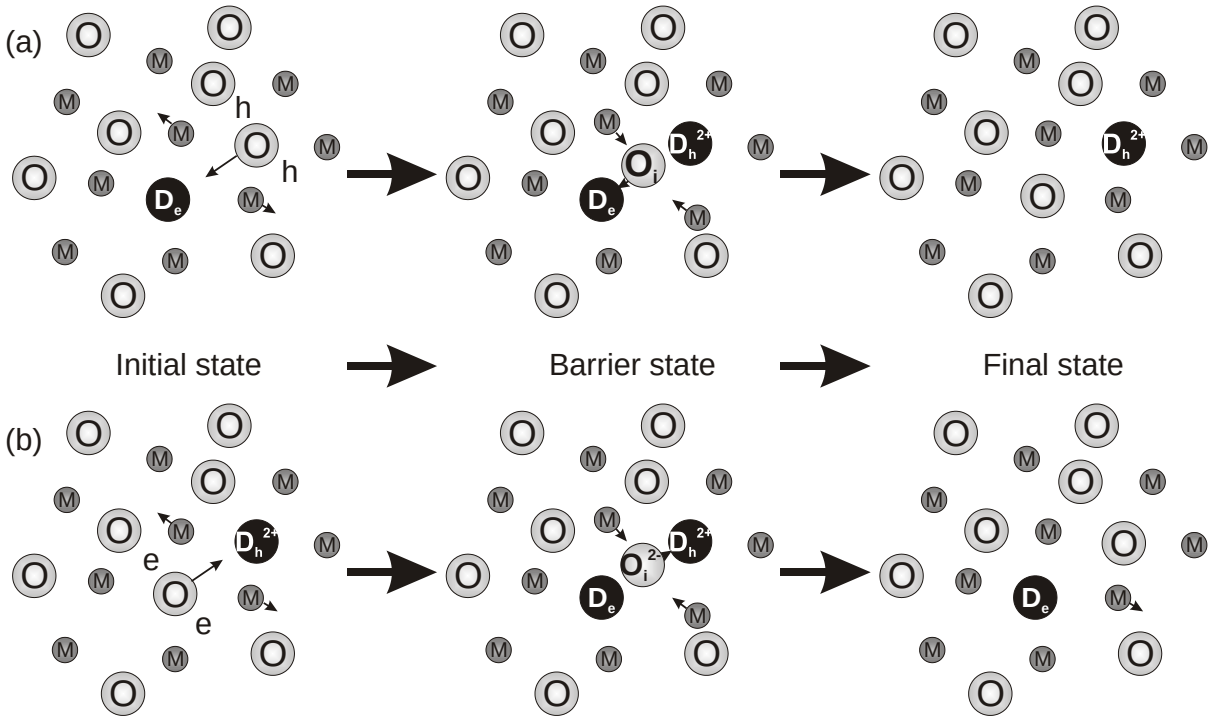

Fig. 4. (a) and (b) are two-dimensional schematic representations of the defect conversion processes in equations 8(a) and 8(b) respectively. Shaded circles with an M and O represent metal and oxygen atoms respectively. When an oxygen atom is in an interstitial state, it is represented by $\mathbf{O_i}$ and any charge state is indicated. Oxygen vacancy states are identified by solid black circles. Arrows indicate that some movement will be taking place. Initial, final and the barrier states are all shown. It is the energy barrier associated with the barrier state (i.e. the oxygen vacancy migration energy) that defines the energy barrier for the process and the resulting metastability.